Mechanics of human brain organoids

Valentina Balbi,[1] Michel Destrade ,[2] and Alain Goriely [3]

[1]*Department of Mathematics and Statistics, University of Limerick, Limerick V94 T9PX, Ireland*
[2]*School of Mathematics, Statistics and Applied Mathematics, NUI Galway, Galway H91 TK33, Ireland*
[3]*Mathematical Institute, University of Oxford, Oxford OX1 2JD, United Kingdom*

Organoids are prototypes of human organs derived from cultured human stem cells. They provide a reliable and accurate experimental model to study the physical mechanisms underlying the early developmental stages of human organs and, in particular, the early morphogenesis of the cortex. Here we propose a mathematical model to elucidate the role played by two mechanisms which have been experimentally proven to be crucial in shaping human brain organoids: the contraction of the inner core of the organoid and the microstructural remodeling of its outer cortex. Our results show that both mechanisms are crucial for the final shape of the organoid and that perturbing those mechanisms can lead to pathological morphologies which are reminiscent of those associated with lissencephaly (smooth brain).

I. INTRODUCTION

The characteristic convoluted shape of the human brain was first reported in the Edwin Smith papyrus, an Egyptian manuscript dated 1700BC that compares brain convolutions to the corrugations or wrinkles found in molten metal [1]. The description, development, and function of these convolutions have also been major topics of research since the early 1800s [2].

The visible upper part of the convolutions are called *gyri* and their deep groves are referred to as *sulci*. Geometrically, the convolutions increase the surface area of the brain for a given volume. From a functional point of view, it is believed that they have the strategic functions of increasing the number of neuronal bodies located in the cortex and of facilitating the connections between neurons and hence reducing the traveling time of electric signals between different regions.

Although different explanations have been proposed, the mechanisms behind *gyrification* are not fully understood. It is now accepted that intrinsic *mechanical forces*, rather than external constraints, are responsible for the emergence of folding in the human brain [3]. Recent observational studies [4,5] further support the role of the rapid tangential expansion of the cortex during development as the primary driver for folding [2,6–9].

At the simplest physical level, the onset of folding can be understood as an initial build up of elastic energy in the compressed upper cortex and its partial release by a wrinkling deformation of the film and substrate. Experimentally, this instability can be observed in the constrained polymeric swelling of a circular shell bounded to an elastic disk which triggers the same type of wrinkling pattern [10–14]. Similar experiments performed on a two-layered brain prototype made of polymeric gels with differential swelling properties reproduce folds similar to the gyri and sulci of a real brain [15].

Yet the human brain is too complex to be used as an experimental platform to unravel the detailed cellular mechanisms leading to folding. An alternative approach is to use *human brain organoids*.

Brain organoids are self-organized and collective structures produced in vitro from the culturing of human stem cells that mimic the early development of the human brain. In particular, when cultured in a mostly flat geometry, these organoids develop wrinkling patterns as shown recently by Karzbrun *et al.* [16] (Fig. 1). Moreover, these authors identified two possible mechanisms for surface folding during cortical development: the contraction of the organoid lumen and the nuclei motion of neuronal progenitor cells within the cortical layer–interkinetic nuclear migration (INM) [17,18].

The cortex is populated by progenitor cells (that will later become neurons) radially oriented across the layer. Their nuclei move up and down across the cells following the cell cycle: first apical-ward (toward the lumen) and then basalward (toward the outer surface of the cortex). Karzbrun *et al.* [16] found that the nuclei accumulate in the basal zone of the cortex. This accumulation induces a swelling in proximity of the outer surface and causes the onset of the wrinkling. Computer simulations and physical arguments were proposed but without fully integrating the remodeling and contraction processes. Alternative models were proposed in Refs. [19,20].

Different morphologies can be obtained by varying these two effects. The key problem is then to develop a physical model to understand the relative role of each effect in creating folding patterns in brain organoids. Here we use *morphoelasticity* [21], the theory of growing and remodeling continua, to model brain organoids and explore various parameter regimes.

II. THE MODEL

The organoid is modeled as a two-dimensional (2D) continuum morphoelastic structure made of an inner disk, the lumen, which serves as the core of the organoid, and a
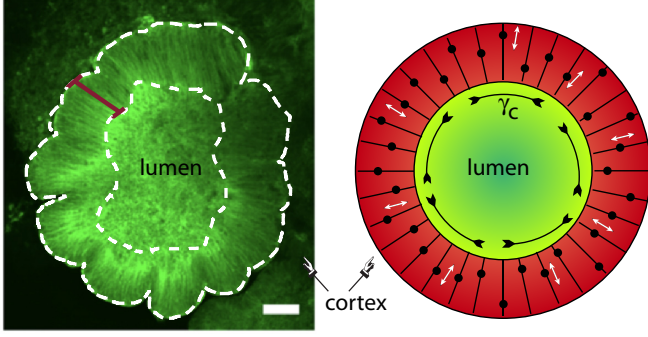
FIG. 1. Left: Morphology of a growing human brain organoid (adapted from Ref. [16], scale bar is 100 μm). Right: A two-dimensional morphoelastic model. The black circles represent the nuclei that move up and down radially while the lumen can contract in the hoop direction.
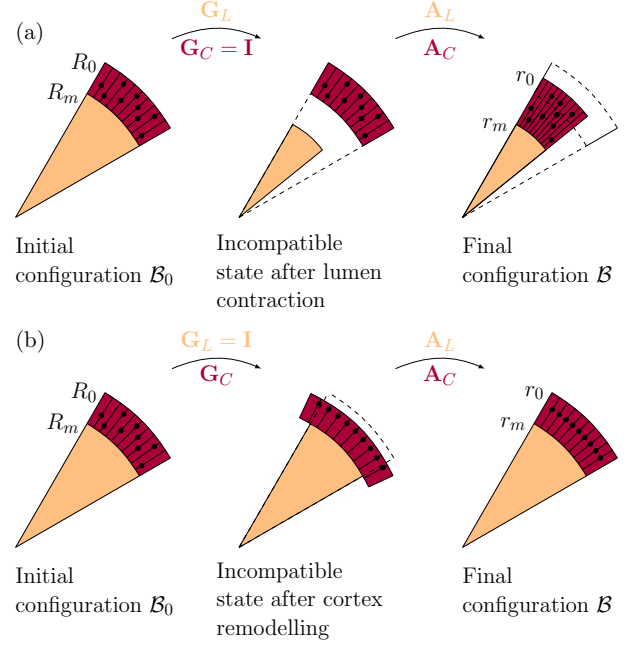

FIG. 2. Schematic illustration of (a) the contraction of the lumen and (b) the remodeling of the cortex (small dots represent nuclei).

surrounding ring, the cortex. We introduce a cylindrical co-ordinate system so that a material point at position $\mathbf{X} \in \mathbb{R}^2$ with components (R, Θ) in the initial configuration $\mathcal{B}_0$ is at position $\mathbf{x} \in \mathbb{R}^2$ with components (r, θ) in the final, deformed, configuration $\mathcal{B}$. The deformation $\mathbf{x} = \mathbf{x}(\mathbf{X})$ from $\mathcal{B}_0$ to $\mathcal{B}$ defines the associated deformation gradient $\mathbf{F} = \partial \mathbf{x}/\partial \mathbf{X}$.

To model the contraction of the lumen (shrinking) and the remodeling of the cortex, we use the multiplicative decomposition of the deformation gradient. Hence $\mathbf{F}$ is split into the product of a tensor $\mathbf{G}$, describing the natural growth or remodeling of the tissue and introducing a virtual intermediate incompatible state, and of an elastic deformation tensor $\mathbf{A}$, restoring the compatibility of the structure, while possibly introducing residual stresses [21].

Specifically, the lumen undergoes a uniform contraction that results in an isotropic shrinking in the plane, while microstructural changes occur at constant volume within the cortex due to the radial motion of cell bodies. The tensor $\mathbf{G}$ for the lumen and the cortex is

$$\mathbf{G}_L = \mathrm{diag}(\gamma_L, \gamma_L) \quad \text{and} \quad \mathbf{G}_C = \mathrm{diag}(\gamma_C, 1/\gamma_C), \quad (1)$$

respectively, where $\gamma_L < 1$ is a measure of the volumetric contraction of the lumen and γ_C is the remodeling stretch associated with microstructural changes in the cortex. Experimentally, γ_L can be assessed by a continuous measurement of the volume and γ_C by following the motion of the nuclei in the cortex.

Figure 2(a) illustrates the deformation resulting from the contraction of the lumen and Fig. 2(b) shows how a slice of the organoid deforms when remodeling occurs in the cortex. This form of $\mathbf{G}_C$ captures the observed back and forth motion of the nuclei of neuron progenitor cells, because it generates inward or outward forces within the cortex, as we show later.

Note that the multiplicative decomposition of the deformation gradient has been extensively employed within the theory of morphoelasticity to model successfully morphogenetic processes in biological soft tissues such as pattern formation in tubular organs and spherical growth [10,22–25]. In those models, the morphological transitions were associated with the onset of an elastic instability generated by differential growth between different tissue layers. The novelty here is

that we elucidate the role played by two distinct biological processes in shaping the brain: on the one hand, the contractile shrinking of the lumen and, on the other hand, the internal remodeling of the cortex.

Both the lumen and the cortex are assumed incompressible and a simple base solution for the deformation maintaining the circular symmetry is

$$\begin{aligned} r = \gamma_L R, \qquad & \theta = \Theta \quad \text{for} \quad R \in [0, R_m) \\ r = \sqrt{R^2 + a}, \quad & \theta = \Theta \quad \text{for} \quad R \in [R_m, R_0], \qquad (2) \end{aligned}$$

where $a = r_m^2 - R_m^2$ is the unique unknown parameter (to be specified from the mechanical equilibrium) and R_m, R_0 (r_m, r_0) are the interface and outer radii in the undeformed (deformed) configuration, respectively. The initial geometry of the structure is defined by the nondimensional aspect ratio $H = R_0/R_m$.

We assume that both the lumen and the cortex follow a hyperelastic, isotropic, and neo-Hookean behavior so that each tissue has a strain energy density in the form $W_N = \mu_N[\mathrm{tr}(\mathbf{A}_N \mathbf{A}_N^T) - 3]/2$ $(N = L, C)$, where μ_L and μ_C are the shear moduli of the lumen and cortex, respectively. The Cauchy stress for each tissue is then $\boldsymbol{\sigma}_N = \mu_N \mathbf{A}_N \mathbf{A}_N^T - p_N \mathbf{I}$, where p_N are the Lagrange multipliers introduced by the constraint of incompressibility and $\mathbf{I}$ is the identity tensor.

The elastic equilibrium problem is given by:

$$\frac{d}{dr}\sigma_{Nrr}(r) + \frac{1}{r}[\sigma_{Nrr}(r) - \sigma_{N\theta\theta}(r)] = 0, \quad N = L, C, \quad (3)$$

with boundary and continuity conditions

$$\sigma_{Crr}(r_0) = 0, \quad \text{and} \quad \sigma_{Lrr}(r_m) = \sigma_{Crr}(r_m). \qquad (4)$$

The solution to (A1) with (4) is

$$\sigma_{Crr}(r) = \int_r^{r_0} \mu \frac{B_{Crr}(r) - B_{C\theta\theta}(r)}{r} dr,$$

$$\sigma_{C\theta\theta}(r) = \mu[B_{C\theta\theta}(r) - B_{Crr}(r)] + \sigma_{Crr}(r),$$

$$\sigma_{Lrr}(r) = \sigma_{Lrr}(r_m), \quad \sigma_{L\theta\theta}(r) = \sigma_{L\theta\theta}(r_m). \tag{5}$$

This solution shows that the Cauchy stress is constant within the lumen because the deformation is homogeneous there (details given in Appendix A). The hoop stress $\sigma_{C\theta\theta}$ is negative within the cortex, indicating that the outer layer is under circumferential compression.

We expect that for some critical values of the parameters, the organoid will buckle to release the build-up of compressive residual stress in the cortex. Further, when $\gamma_C < 1$ a positive radial stress is generated and the force gradient favors the outward nuclei motion. When $\gamma_C > 1$ the radial stress component is negative and contributes to pushing the nuclei inwardly, according to the observed cyclic outward or inward nuclear motion within the cortex.

Next we study the stability of the symmetric solution in (2) and (A3). We perturb the current position vector $\mathbf{x}$ with components in (2) by superposing an incremental [26] deformation $\delta\mathbf{x}$. The perturbed position vector is $\tilde{\mathbf{x}}_N = \mathbf{x}_N + \varepsilon\delta\mathbf{x}_N$ ($N = L, C$), where ε is small, and the associated elastic deformation gradient is $\tilde{\mathbf{A}}_N = \mathbf{A}_N + \varepsilon\mathbf{\Gamma}_N\mathbf{A}_N$, where $\mathbf{\Gamma}_N = \partial\delta\mathbf{x}_N/\partial\mathbf{x}_N$ is the incremental displacement gradient. Accordingly, we define the perturbed stress $\tilde{\boldsymbol{\sigma}}_N = \boldsymbol{\sigma}_N + \varepsilon\delta\boldsymbol{\sigma}_N$ where:

$$\delta\boldsymbol{\sigma}_N = \mathcal{A}_N : \mathbf{\Gamma}_N^T + p_N\delta\mathbf{F}_N - \delta p_N\mathbf{I} \tag{6}$$

is the push-forward of the incremental nominal stress. Here $\mathcal{A}_N = \mathbf{A}_N(\partial^2 W_N/\partial\mathbf{A}_N^2)\mathbf{A}_N$ is the fourth-order tensor of the instantaneous elastic moduli and δp_N is the increment of the Lagrange multiplier. Note that $\mathcal{A}_L$ is constant because the deformation is homogenous within the lumen. The incremental problem then amounts to solving

$$\text{div}\,\delta\boldsymbol{\sigma}_N = \mathbf{0} \quad \text{and} \quad \text{tr}\,\mathbf{\Gamma}_N = 0, \quad N = \{L, C\} \tag{7}$$

the latter being the incremental incompressibility condition.

We seek a wrinkling solution of the form:

$$\{\delta r_N, \delta p_N\} = \{U_N(r), P_N(r)\}\cos(m\theta)$$

$$\delta\theta_N = V_N(r)\sin(m\theta), \tag{8}$$

where $\delta r_N, \delta\theta_N$ are the components of the incremental displacement $\delta\mathbf{x}_N$ and m is the wave number of the perturbation.

To tackle the incremental problem (7), which is a second-order linear system of three partial differential equations with boundary conditions, we transform it into a first-order linear system of four ordinary differential equations (ODEs) with initial conditions. From (7) and (8) we find that the incremental stress components have the forms: $(\delta\boldsymbol{\sigma}_N)_{rr} = \Sigma_{Nrr}(r)\cos(m\theta)$ and $(\delta\boldsymbol{\sigma}_N)_{r\theta} = \Sigma_{Nr\theta}(r)\sin(m\theta)$ and we rewrite (7) as

$$\frac{d}{dr}\boldsymbol{\eta}_N(r) = \frac{1}{r}\mathbf{M}_N(r)\boldsymbol{\eta}_N(r), \quad N = \{L, C\}, \tag{9}$$

where $\boldsymbol{\eta}_N(r) = \{U_N(r), r\Sigma_N(r)\}^T$ and the 4×4 $\mathbf{M}_N$ is the so-called Stroh matrix [27–30]. Note that (9) is a system of ODEs with variable coefficients.
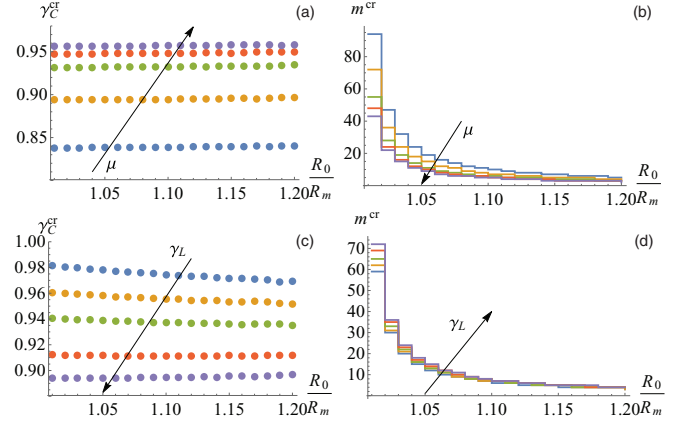

FIG. 3. Critical instability threshold γ_C^{cr} and wave number m^{cr} against the initial aspect ratio $H = R_0/R_m$ at varying stiffness ratios $\mu_C/\mu_L = \{5, 10, 20, 30, 40\}$ with fixed $\gamma_L = 1$ [(a) and (b)] and at varying $\gamma_L = \{0.91, 0.93, 0.95, 0.98, 1\}$ with fixed $\mu = 10$ [(c) and (d)].

In the lumen, because $\mathbf{M}_L$ has constant components, we have:

$$\boldsymbol{\eta}_L(r) = c_1 r^{m-1}\boldsymbol{\eta}^{(1)}(r) + c_2 r^{m+1}\boldsymbol{\eta}^{(2)}(r), \tag{10}$$

where $m-1$ and $m+1$ are the eigenvalues of $\mathbf{M}_L$ and $\boldsymbol{\eta}^{(i)}(r) = \{\boldsymbol{\eta}_{Ui}(r), \boldsymbol{\eta}_{\Sigma i}(r)\}^T$ with $i = \{1, 2\}$ are the associated eigenvectors.

To solve numerically the Stroh problem in the cortex (method given in Appendices B and C), we fix H and μ, and by iterating over the wave number m and either γ_C or γ_L, we solve for $\boldsymbol{\eta}$ from r_0 to r_m with null initial condition until the outer boundary conditions are satisfied.

III. RESULTS

Figure 3 shows the critical instability thresholds of the cortex remodeling stretch γ_C^{cr} against the initial aspect ratio R_0/R_m at varying lumen volumetric changes γ_L and varying stiffness ratios μ_C/μ_L with the associated critical wave number m^{cr}.

From Figs. 3(a) and 3(b) we conclude that the stiffer the cortex, the higher the critical remodeling thresholds γ_C^{cr}. Therefore, disks with a stiff ring will buckle earlier (in the sense that the remodeling in the cortex introduces less circumferential compression to trigger the instability) than those with a soft ring. These results are in accordance with those found for a substrate with a growing layer [31].

Another interesting aspect arises from Fig. 3(a): When the lumen does not contract ($\gamma_L = 1.0$), the cortex instability thresholds γ_C^{cr} are independent of the initial thickness of the cortical ring, i.e., the aspect ratio H. However, the instability patterns [m^{cr} in Fig. 3(b)] do depend on the thickness of the cortex (particularly for very thin rings).

Finally, as the lumen contracts [upper curves in Fig. 3(c), $\gamma_L < 1$], the critical thresholds γ_C^{cr} for the cortex decrease, indicating that the more the lumen contracts, the earlier the cortex will buckle. This behavior is expected from the mechanics viewpoint, because lumen contraction leads to a compressive circumferential stress in the cortex.
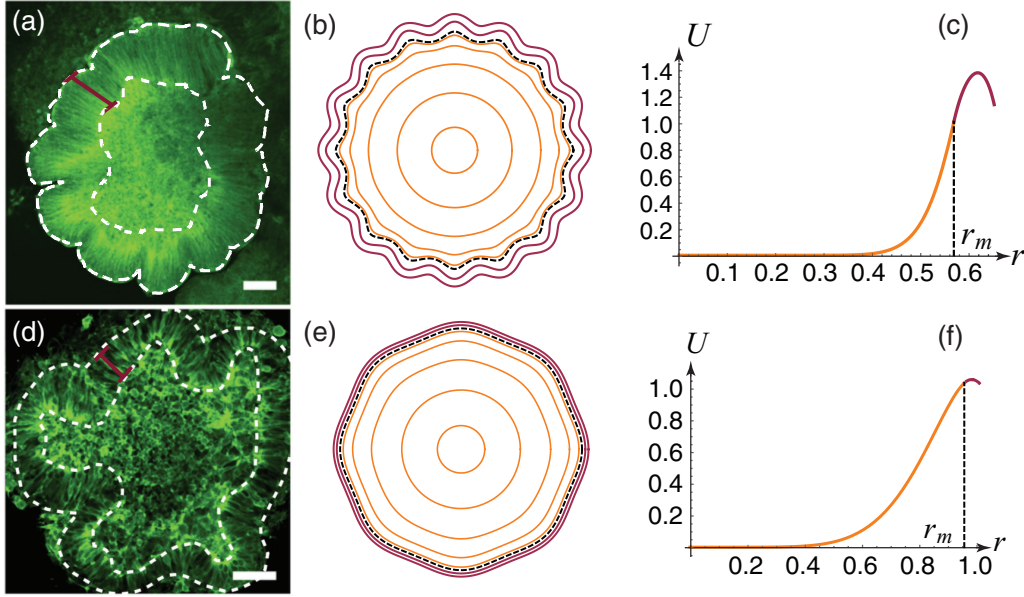
FIG. 4. Effect of contraction inhibition on the final morphology of the organoid: [(a) and (d)] control and drug-treated organoids (digitized from Ref. [16], scale bars are 100 μm); [(b) and (e)] instability patterns predicted by our model from an initial organoid with $H = 1.05$, $\gamma_C = 1$ and by setting $\mu_C/\mu_L = 0.85$ in (b), and $\mu_C/\mu_L = 40$ in (e); [(c) and (f)] magnitude of the incremental displacements $U_N(r)$, $V_N(r)$, $(N = L, C)$ within the organoid (orange and purple, respectively), computed using the same parameters as in (b) and (e) and taking $\varepsilon = 0.02$.

In Fig. 4, we show the final morphologies obtained from two disks with the same initial aspect ratio $H = 1.05$ but with different stiffness ratios μ. In Fig. 4(e) the lumen is softer than the cortex ($\mu_C/\mu_L = 40$) and the opposite scenario is modeled in Fig. 4(b) ($\mu_C/\mu_L = 0.85$). The critical threshold for the instability in Fig. 4(e): $\gamma_L^{cr} = 0.95$ is much higher than that in Fig. 4(b), $\gamma_L^{cr} = 0.57$, indicating that disks with softer cores buckle at lower contraction thresholds.

IV. DISCUSSION

These results are able to capture the effect of contraction inhibition of the cytoskeleton observed in human organoids. Indeed, in Ref. [16] organoids treated with Blebbistatin (a drug used to reduce the contractility of the lumen) were found to have a softer core [Case (e)] than control organoids [Case (b)]. Moreover, our model predicts that the critical wave number for a disk with a soft core, $m^{cr} = 8$, is lower than that of a disk with a stiffer core, $m^{cr} = 16$. Hence our model predicts the experimental result that treated organoids display less folds than control ones [compare Figs. 4(a) and 4(b) with Figs. 4(d) and 4(e)]. This is in line with results obtained by differential growth models where both the lumen and the ring grow but at different rates [14]. By contrast in our study, the lumen and the ring undergo two different mechanisms: The former contracts and the latter remodels according to the INM.

Furthermore, by comparing the magnitude of the instability patterns in Figs. 4(c) and 4(f) we can observe that in Case (b) (hard lumen), the pattern is more pronounced at the outer radius r_0 than at the contact radius r_m, whereas in Case (e) (soft lumen) the trend of the magnitude is reversed. The model thus encapsulates the experimental observation that when the contractility of the organoid is disrupted, the apical surface

(i.e., the interface between the lumen and the cortex) corrugates more than the basal one (outer surface of the organoid).

Our model also predicts the experimentally observed linear scaling law between the critical wavelength λ^{cr} and the initial thickness t of the cortex, in agreement with previous models [32,33]. In Fig. 5, we compare quantitatively the predictions of our model with the data reported in Ref. [16] for the LIS1 $+/-$ mutation. In the thickness range 50–150 mm, Karzbrun *et al.* [16] report linear factors (slopes) between the wavelength and the thickness for the control and the mutant organoids of amounts 0.8 and 1.9, respectively. Moreover, they find that the LIS1 $+/-$ mutation induces a reduction of the lumen stiffness by a factor 2. To validate our model, we calculate the predicted wavelength of the instability pattern for disks with stiffness ratio $\mu_C/\mu_L = 0.48$ (blue line) and for disks with halved lumen stiffness μ_L, i.e., $\mu_C/\mu_L = 0.9$ (orange line). The slopes predicted by our models are 0.75 (blue line, obtained by setting $\mu_C/\mu_L = 0.48$) and 1.93 (orange line, obtained by halving the lumen ratio, so that $\mu_C/\mu_L = 0.9$), showing good agreement with the experimental observations.

Furthermore, the LIS1 mutation not only softens the lumen of the organoid, but it also slows the inward motion of the nuclei. This leads to an accumulation of nuclei at the outer surface of the cortex and introduces a compression along the circumference of the cortical ring. In effect, our model predicts that for disks with stiffness ratio $\mu_C/\mu_L = 0.9$ (orange points, mutant), the critical remodeling threshold of the cortex $\gamma_C^{cr} = 0.61$ is higher (i.e., buckling occurs earlier) than for the case $\mu_C/\mu_L = 0.48$ (blue line, control) where $\gamma_C^{cr} = 0.54$ [see Fig. 5(b)]. Therefore, our model accurately predicts the effect of the LIS1 mutation of reducing the stiffness of the lumen and perturbing the INM.
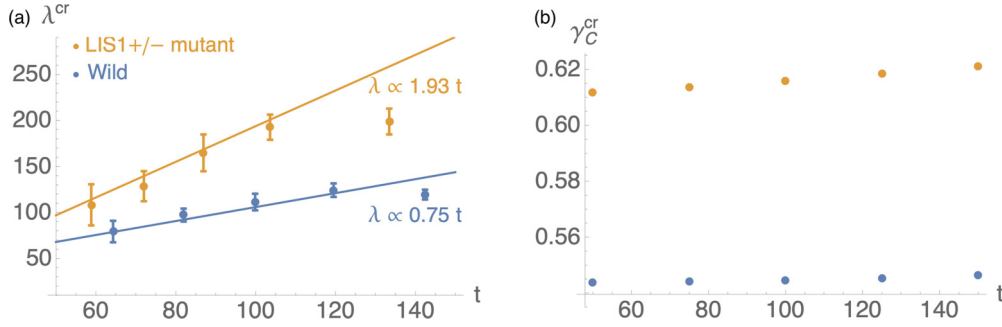
FIG. 5. LIS1 + /− mutation. (a) Wavelength λ of the instability pattern vs initial thickness t of the cortical layer. Data with error bars (reproduced from Ref. [16]) and our model predictions (lines) for control [blue (dark grey)] and for LIS1 + /− mutant organoids [orange (light grey)]; the blue line is obtained by setting $\mu_C/\mu_L = 0.48$ and the orange line by setting $\mu_C/\mu_L = 0.9$. The slopes of the two lines are also shown (the offsets are discarded for a proper visual display). The last data points of each set are considered as outliers [16]. (b) Associated instability thresholds for the cortex remodeling parameter γ_C^{cr}.

V. CONCLUSION

Our model predicts the onset of wrinkling in human brain organoids, usually associated with the early gyrification in the human brain. We find that both the contraction of the lumen and the motion of the nuclei of neuron progenitor cells within the cortex play a crucial role in the early stages of brain development. Disruption of any of these mechanisms results in alteration of the final folding pattern and leads to brain malformation.

In particular, this model gives new insights on the role played by the microstructural remodeling of the cortex in determining the lissencephaly pathology, a mutation associated with a smoother cortex.

Our results suggest that a reduced contractility of the core and a slower motion of nuclei both induce a delay in the onset of the instability and trigger a smoother instability pattern. This model and recent works on brain mechanics further emphasize the crucial role of mechanical forces in brain development and function [34].

APPENDIX A: THE STRESS PROFILE OF THE RADIALLY SYMMETRIC SOLUTION

As shown in the main text, the elastic equilibrium problem is given by:

$$\frac{d}{dr}\sigma_{Nrr}(r) + \frac{\sigma_{Nrr}(r) - \sigma_{N\theta\theta}(r)}{r} = 0, \quad N = \{L, C\} \quad (A1)$$

with

$$\sigma_{Crr}(r_0) = 0 \quad \text{and} \quad \sigma_{Lrr}(r_m) = \sigma_{Crr}(r_m). \quad (A2)$$

The solution to (A1) and (A2) is

$$\sigma_{Crr}(r) = \int_r^{r_0} \mu \frac{B_{Crr}(r) - B_{C\theta\theta}(r)}{r} dr, \quad (A3)$$

$$\sigma_{C\theta\theta}(r) = \mu[B_{C\theta\theta}(r) - B_{Crr}(r)] + \sigma_{Crr}(r), \quad (A4)$$

$$\sigma_{Lrr}(r) = \sigma_{Lrr}(r_m), \quad (A5)$$

$$\sigma_{L\theta\theta}(r) = \sigma_{L\theta\theta}(r_m). \quad (A6)$$

The solution is shown in Fig. 6 in two scenarios: [Fig. 6(a)] growth of the lumen and [Figs. 6(b) and 6(c)] remodeling of the cortex. In the first two cases, the circumferential stress is negative within the cortex, indicating that the outer layer is under circumferential compression. Figures 6(b) and 6(c) also show that when $\gamma_C < 1$ a positive radial stress is generated and the force gradient favors the outward nuclei motion. On the other hand, when $\gamma_C > 1$ the radial stress component is negative and contributes to pushing the nuclei inwardly, according to the observed cyclic outward or inward nuclear motion within the cortex.

APPENDIX B: THE STROH FORMULATION

The Stroh formalism is an analytical technique that allows to transform the incremental problem (a system of four partial differential equations (PDEs) with boundary conditions) into a system of six ODEs with initial conditions. It is based on the assumption that the incremental displacements $\delta\mathbf{x}_N = (\delta r_N, \delta\theta_N)^T$, the incremental stress components $(\delta\boldsymbol{\sigma}_N)_{rr}, (\delta\boldsymbol{\sigma}_N)_{r\theta}$ and the Lagrange multiplier δp_N can be written in the separable form:

$$(\delta r_N, \delta p_N, (\delta\boldsymbol{\sigma}_N)_{rr}) = (U_N(r), P_N(r), \Sigma_{Nrr}(r))\cos(m\theta)$$
$$(\delta\theta_N, (\delta\boldsymbol{\sigma}_N)_{r\theta}) = (V_N(r), \Sigma_{Nr\theta}(r))\sin(m\theta) \quad (B1)$$

with $N = \{L, C\}$. Then the incremental problem takes the following form:

$$\frac{d\boldsymbol{\eta}_N(r)}{dr} = \frac{1}{r}\mathbf{M}_N(r)\boldsymbol{\eta}_N(r), \quad N = \{L, C\}, \quad (B2)$$

where $\boldsymbol{\eta}_N(r) = (\mathbf{U}_N(r), r\boldsymbol{\Sigma}_N(r))^T$, $\mathbf{U}_N(r) = (U_N(r), V_N(r))^T$ is the displacement vector, and $\boldsymbol{\Sigma}_N(r) = (\Sigma_{Nrr}(r), \Sigma_{Nr\theta}(r))^T$ is the traction vector and the 4×4 block-matrix $\mathbf{M}_N$ is the
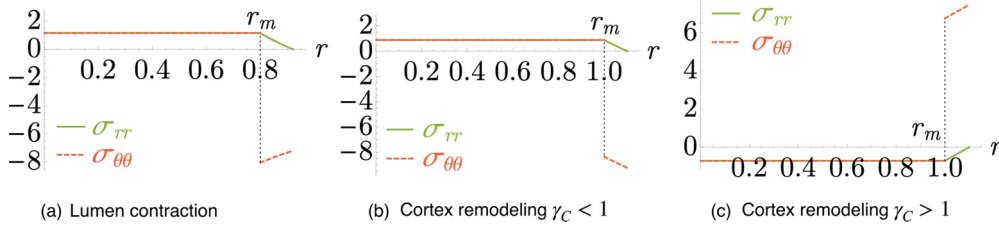
FIG. 6. Axial-symmetric solution to the elastic problem in Eqs. (A1) and (A2). The radial (green solid) and circumferential (red dashed) components of the Cauchy stress. (a) The lumen undergoes contraction: $\gamma_L = 0.8$, $\gamma_C = 1$. [(b) and (c)] The cortex undergoes remodeling: $\gamma_L = 1$, $\gamma_C = 0.8$ (b) and $\gamma_C = 1.2$ (c). The aspect ratio and the stiffness ratio are fixed: $H = 1.1$, $\mu_C/\mu_L = 10$.

so-called Stroh matrix. Within the lumen, we have

$$\frac{d\boldsymbol{\eta}_L(r)}{dr} = \frac{1}{r}\mathbf{M}_L(r)\boldsymbol{\eta}_L(r), \quad \lim_{r \to 0}\mathbf{U}_L(r) = \mathbf{0}, \tag{B3}$$

where the Stroh matrix has the following block-form:

$$\mathbf{M}_L = \begin{pmatrix} \mathbf{M}_{L1} & \mathbf{M}_{L2} \\ \mathbf{M}_{L3} & -\mathbf{M}_{L1}^T \end{pmatrix} \tag{B4}$$

with

$$\mathbf{M}_{L1} = \begin{pmatrix} -1 & -m \\ m[1 - \sigma_{Crr}(r_m)/\mu_L] & 1 - \sigma_{Crr}(r_m)/\mu_L \end{pmatrix}, \qquad \mathbf{M}_{L2} = \begin{pmatrix} 0 & 0 \\ 0 & 1/\mu_L \end{pmatrix},$$

$$\mathbf{M}_{L3} = \begin{pmatrix} -[\sigma_{Crr}(r_m) - 2\mu_L][m^2\sigma_{Crr}(r_m) + 2\mu_L]/\mu_L & -m[\sigma_{Crr}^2(r_m) - 4\mu_L] \\ -m[\sigma_{Crr}(r_m)^2 - 4] & -[\sigma_{Crr}(r_m) - 2][\sigma_{Crr}(r_m) + 2m^2] \end{pmatrix}. \tag{B5}$$

We note that the blocks in Eq. (B5) are independent on r, and therefore Eq. (B3) becomes an ODE with constant coefficients and its solution can be written in terms of the eigenvalues and eigenvectors of $\mathbf{M}_L$. Now $\mathbf{M}_L$ has four eigenvalues: $m \pm 1$ and $-m \pm 1$, and thus the solution has the following form:

$$\boldsymbol{\eta}_L(r) = c_1 \boldsymbol{\eta}^{(1)}(r)r^{m-1} + c_2 \boldsymbol{\eta}^{(2)}(r)r^{m+1} + c_3 \boldsymbol{\eta}^{(3)}(r)r^{-m-1} + c_4 \boldsymbol{\eta}^{(4)}(r)r^{-m+1}, \tag{B6}$$

where $\boldsymbol{\eta}^{(i)}(r)$, $i = \{1, \ldots, 4\}$ are the eigenvectors of $\mathbf{M}_L$. We discard the mode $m = 1$ for which the matrix $\mathbf{M}_L$ has a repeated eigenvalue, indicating the presence of rigid body motions. For $m \geqslant 2$ we can then use the fact that the perturbation must decay with $r \to 0$ (thus c_3 and c_4 must be zero) so that (B6) reduces to:

$$\boldsymbol{\eta}_L(r) = c_1 \boldsymbol{\eta}^{(1)}(r)r^{m-1} + c_2 \boldsymbol{\eta}^{(2)}(r)r^{m+1} = \begin{pmatrix} \boldsymbol{\eta}_{U1}(r) & \boldsymbol{\eta}_{U2}(r) \\ \boldsymbol{\eta}_{\Sigma1}(r) & \boldsymbol{\eta}_{\Sigma2}(r) \end{pmatrix} \begin{pmatrix} c_1 r^{m-1} \\ c_2 r^{m+1} \end{pmatrix}, \tag{B7}$$

where $\boldsymbol{\eta}^{(i)} = \{\boldsymbol{\eta}_{Ui}(r), \boldsymbol{\eta}_{\Sigma i}(r)\}^T$, $i = \{1, 2\}$ and $\boldsymbol{\eta}_{Ui}(r)$ and $\boldsymbol{\eta}_{\Sigma i}(r)$ are 2×1 (column) vectors containing the displacement and the traction components, respectively, of the eigenvector $\boldsymbol{\eta}^{(i)}$.

Within the cortex, the Stroh problem is written as follows:

$$\frac{d\boldsymbol{\eta}_C(r)}{dr} = \frac{1}{r}\mathbf{M}_C(r)\boldsymbol{\eta}_C(r), \tag{B8}$$

with initial conditions:

$$\boldsymbol{\eta}_C(r_m) = \boldsymbol{\eta}_L(r_m), \tag{B9}$$

$$\boldsymbol{\Sigma}_C(r_0) = \mathbf{0}. \tag{B10}$$

Equation (B9) is the continuity condition at the interface between the lumen and the cortex, and Eq. (B10) imposes a traction-free condition at r_0. The blocks of the Stroh matrix $\mathbf{M}_C$ in Eq. (B8) are given by:

$$\mathbf{M}_{C1} = \begin{pmatrix} -1 & -m \\ \frac{m\,p_C(r)}{\mathcal{A}_{Cr\theta r\theta}(r)} & \frac{p_C(r)}{\mathcal{A}_{Cr\theta r\theta}(r)} \end{pmatrix}, \quad \mathbf{M}_{C2} = \begin{pmatrix} 0 & 0 \\ 0 & \frac{1}{\mathcal{A}_{Cr\theta r\theta}(r)} \end{pmatrix},$$

$$\mathbf{M}_{C3} = \begin{pmatrix} \alpha_C(r) + m^2\mathcal{A}_{C\theta r\theta r}(r) - \frac{p_C^2(r)m^2}{\mathcal{A}_{Cr\theta r\theta}(r)} & m[\alpha_C(r) + \mathcal{A}_{C\theta r\theta r}(r)] - \frac{m\,p_C^2(r)}{\mathcal{A}_{Cr\theta r\theta}(r)} \\ m[\alpha_C(r) + \mathcal{A}_{C\theta r\theta r}(r)] - \frac{m\,p_C^2(r)}{\mathcal{A}_{Cr\theta r\theta}(r)} & m^2\alpha_C(r) + \mathcal{A}_{C\theta r\theta r}(r) - \frac{p_C^2(r)}{\mathcal{A}_{Cr\theta r\theta}(r)} \end{pmatrix} \tag{B11}$$

and $\mathbf{M}_{C4} = -\mathbf{M}_{C1}^T$, where we have defined $\alpha_C(r) = \mathcal{A}_{Crrrr}(r) + \mathcal{A}_{C\theta\theta\theta\theta}(r) + 2p_C(r)$. In summary, the solution to the Stroh problem within the lumen has the form of Eq. (B7). However, to solve the problem within the cortex we need to implement a robust numerical scheme. Since the initial conditions in Eq. (B10) are on the stress components, numerical stiffness issues arise and standard numerical techniques fail to converge. Therefore, we use the impedance matrix method which allows to implement a robust and stable numerical procedure.

APPENDIX C: THE IMPEDANCE METHOD AND THE RICCATI EQUATION

We introduce the conditional impedance matrix $\mathbf{Z}_N(r, r_i)$, $N = \{L, C\}$ which is related to the displacement and traction vectors through:

$$\mathbf{Z}_N(r, r_i)\mathbf{U}_N(r) = r\mathbf{\Sigma}_N(r), \quad N = \{L, C\}. \quad (C1)$$

The term *conditional* refers to the fact that the impedance matrix depends on the condition at r_i. We now transform the general form of the Stroh problem in Eq. (B2) into the Riccati equation. On substituting (C1) into (B2), we obtain:

$$\frac{d\mathbf{U}_N}{dr} = \frac{1}{r}(\mathbf{M}_{N1}\mathbf{U}_N + \mathbf{M}_{N2}\mathbf{Z}_N\mathbf{U}_N), \quad (C2)$$

$$\frac{d(\mathbf{Z}_N\mathbf{U}_N)}{dr} = \frac{1}{r}\left(\mathbf{M}_{N3}\mathbf{U}_N - \mathbf{M}_{N1}^T\mathbf{Z}_N\mathbf{U}_N\right). \quad (C3)$$

By differentiating and substituting (C2) into (C3) we get the Riccati equation:

$$r\frac{d\mathbf{Z}_N}{dr} = -\mathbf{Z}_N\mathbf{M}_{N1} - \mathbf{Z}_N\mathbf{M}_{N2}\mathbf{Z}_N + \mathbf{M}_{N3} - \mathbf{M}_{N1}^T\mathbf{Z}_N. \quad (C4)$$

Now we choose to use the conditional impedance matrix $\mathbf{Z}_C(r, r_0)$, which is obtained by integrating Eq. (C4) within the cortex from r_0 to r_m, using the initial condition at r_0 which [from (B10)] is written as follows:

$$\mathbf{Z}_C(r_0, r_0) = \mathbf{0}. \quad (C5)$$

By using (B9), the continuity condition of the traction vector reads:

$$r_m\mathbf{\Sigma}_L(r_m) = r_m\mathbf{\Sigma}_C(r_m) = \mathbf{Z}_C(r_m, r_0)\mathbf{U}_C(r_m)$$
$$= \mathbf{Z}_C(r_m, r_0)\mathbf{U}_L(r_m) \quad (C6)$$

and then by substituting Eq. (B7), Eq. (C6) reduces to:

$$\det[(\boldsymbol{\eta}_{\Sigma 1}(r_m), \boldsymbol{\eta}_{\Sigma 2}(r_m)) - \mathbf{Z}_C(r_m, r_0)(\boldsymbol{\eta}_{U1}(r_m), \boldsymbol{\eta}_{U2}(r_m))] = 0. \quad (C7)$$

For fixed values of H and μ, we generate two iterative loops over γ_N (either γ_C or γ_L) and m. Inside the two loops we integrate (C4) with the initial condition (C5), until the stop condition (C7) is satisfied. This algorithm allows to get the critical thresholds γ_N^{cr} of the instability and the associated wave numbers m^{cr}.

[1] J. Bearsted, *The Edwin Smith Surgical Papyrus* (University of Chicago Press, Chicago, IL, 1930), Vol. 1.

[2] A. Goriely, S. Budday, and E. Kuhl, Adv. Appl. Mech. **48**, 79 (2015).

[3] G. F. Striedter, S. Srinivasan, and E. S. Monuki, Annu. Rev. Neurosci. **38**, 291 (2015).

[4] L. Ronan, N. Voets, C. Rua, A. Alexander-Bloch, M. Hough, C. Mackay, T. J. Crow, A. James, J. N. Giedd, and P. C. Fletcher, Cereb. Cortex **24**, 2219 (2013).

[5] K. E. Garcia, E. C. Robinson, D. Alexopoulos, D. L. Dierker, M. F. Glasser, T. S. Coalson, C. M. Ortinau, D. Rueckert, L. A. Taber, D. C. Van Essen *et al.*, Proc. Natl. Acad. Sci. USA **115**, 3156 (2018).

[6] D. P. Richman, R. M. Stewart, J. W. Hutchinson, and V. S. Caviness, Science **189**, 18 (1975).

[7] P. V. Bayly, L. A. Taber, and C. D. Kroenke, J. Mech. Behav. Biomed. Mater. **29**, 568 (2014).

[8] S. Budday, P. Steinmann, and E. Kuhl, J. Mech. Phys. Solids **72**, 75 (2014).

[9] P. Bayly, R. Okamoto, G. Xu, Y. Shi, and L. Taber, Phys. Biol. **10**, 016005 (2013).

[10] D. E. Moulton and A. Goriely, J. Mech. Phys. Solids **59**, 525 (2011).

[11] J. Dervaux and M. Ben Amar, J. Mech. Phys. Solids **59**, 538 (2011).

[12] P. Ciarletta, V. Balbi, and E. Kuhl, Phys. Rev. Lett. **113**, 248101 (2014).

[13] V. Balbi, E. Kuhl, and P. Ciarletta, J. Mech. Phys. Solids **78**, 493 (2015).

[14] F. Jia, S. P. Pearce, and A. Goriely, Phys. Rev. E **98**, 033003 (2018).

[15] T. Tallinen, J. Y. Chung, F. Rousseau, N. Girard, J. Lefèvre, and L. Mahadevan, Nat. Phys. **12**, 588 (2016).

[16] E. Karzbrun, A. Kshirsagar, S. R. Cohen, J. H. Hanna, and O. Reiner, Nat. Phys. **1**, 515 (2018).

[17] M. A. Lancaster, M. Renner, C.-A. Martin, D. Wenzel, L. S. Bicknell, M. E. Hurles, T. Homfray, J. M. Penninger, A. P. Jackson, and J. A. Knoblich, Nature **501**, 373 (2013).

[18] T. Miyata, M. Okamoto, T. Shinoda, and A. Kawaguchi, Front. Cell. Neurosci. **8**, 473 (2015).

[19] T. A. Engstrom, T. Zhang, A. K. Lawton, A. L. Joyner, and J. M. Schwarz, Phys. Rev. X **8**, 041053 (2018).

[20] D. Riccobelli and G. Bevilacqua, J. Mech. Phys. Solids **134**, 103745 (2020).

[21] A. Goriely, *The Mathematics and Mechanics of Biological Growth* (Springer Verlag, New York, 2017).

[22] D. E. Moulton and A. Goriely, J. Appl. Physiol. **110**, 1003 (2011).

[23] A. Goriely and M. B. Amar, Phys. Rev. Lett. **94**, 2284 (2005).

[24] Y. Cao, Y. Jiang, B. Li, and X. Feng, Acta Mech. Solida Sin. **25**, 483 (2012).

[25] P. Ciarletta, Phys. Rev. Lett. **110**, 158102 (2013).

[26] M. Ben Amar and A. Goriely, J. Mech. Phys. Solids **53**, 2284 (2005).

[27] A. Goriely, R. Vandiver, and M. Destrade, Proc. Roy. Soc. Lond. A **464**, 3003 (2008).

[28] M. Destrade, J. Acoust. Soc. Am. **109**, 1398 (2001).

[29] M. Destrade, A. Ní Annaidh, and C. Coman, Int. J. Solids Struct. **46**, 4322 (2009).

[30] A. N. Norris and A. Shuvalov, Q. J. Mech. Appl. Math. **63**, 401 (2010).

[31] S. Budday, P. Steinmann, A. Goriely, and E. Kuhl, Extreme Mech. Lett. **4**, 193 (2015).

[32] L. Jin, Y. Liu, and Z. Cai, Int. J. Eng. Sci. **128**, 31 (2018).

[33] H. Alawiye, E. Kuhl, and A. Goriely, Phil. Trans. Roy. Soc. A **377**, 20180076 (2019).

[34] A. Goriely, M. G. D. Geers, G. A. Holzapfel, J. Jayamohan, A. Jérusalem, S. Sivaloganathan, W. Squier, J. A. W. van Dommelen, S. L. Waters, and E. Kuhl, Biomech. Model. Mechanobiol. **14**, 931 (2015).